Tropical forcing of the Summer East Atlantic pattern

C. Ole Wulff[1,3], Richard J. Greatbatch[1,2], Daniela I.V. Domeisen[3], Gereon Gollan[1], Felicitas Hansen[1]

Ole Wulff, ole.wulff@env.ethz.ch

[1]GEOMAR Helmholtz Centre for Ocean Research Kiel, Kiel, Germany

[2]University of Kiel, Kiel, Germany

[3]Institute for Atmospheric and Climate Science, ETH Zurich, Zurich, Switzerland

This article has been accepted for publication and undergone full peer review but has not been through the copyediting, typesetting, pagination and proofreading process, which may lead to differences between this version and the Version of Record. Please cite this article as doi: 10.1002/2017GL075493

The Summer East Atlantic (SEA) mode is the second dominant mode of summer low-frequency variability in the Euro-Atlantic region. Using reanalysis data, we show that SEA-related circulation anomalies significantly influence temperatures and precipitation over Europe. We present evidence that part of the interannual SEA variability is forced by diabatic heating anomalies of opposing signs in the tropical Pacific and Caribbean that induce an extratropical Rossby wave train. This precipitation dipole is related to SST anomalies characteristic of the developing ENSO phases. Seasonal hindcast experiments forced with observed sea surface temperatures (SST) exhibit skill at capturing the interannual SEA variability corroborating the proposed mechanism and highlighting the possibility for improved prediction of boreal summer variability. Our results indicate that tropical forcing of the SEA likely played a role in the dynamics of the 2015 European heat wave.

Keypoints:

- Identification of a 2nd mode of summer variability in the Euro-Atlantic sector
- This SEA mode is forced by tropical diabatic heating anomalies related to the developing ENSO phase
- This tropical-extratropical teleconnection likely played a role in the 2015 European summer heat wave

1. Introduction

Since the early 2000s, summers that were exceptional in terms of temperature and precipitation have occurred more frequently [*Coumou and Rahmstorf*, 2012]. The heat waves of 2003 [*Black et al.*, 2004], 2010 [*Dole et al.*, 2011], and 2015 [*Dong et al.*, 2016] are but three examples. Since these extreme events of significant societal impact occur under preferred atmospheric regimes, it is vital to gain insight into the patterns of the large-scale summer circulation and its prediction.

The dominant summer low-frequency variability mode in the North Atlantic-European (NAE) region is the Summer North Atlantic Oscillation (SNAO) [*Hurrell and Deser*, 2009]. SNAO-related circulation anomalies exert a strong control on precipitation and surface temperature over Europe and eastern North America [*Folland et al.*, 2009]. There are indications that during the positive SNAO phase the frequency of extreme warm days over central Europe is enhanced [*Cassou et al.*, 2005]. Unfortunately, influences on the SNAO useful for predictability on interannual time scales are unclear [*Wulff*, 2017]. For instance, *Folland et al.* [2009] show that the influence of ENSO on interannual SNAO variability is weak.

Compared to the SNAO, other modes of atmospheric summer variability have received relatively little attention. *Cassou et al.* [2005] find a regime in addition to the SNAO related to exceptionally high temperatures over France. They refer to this regime as the Atlantic Low (AL) pattern since it is characterized by a large cyclonic anomaly with its

center over the North Atlantic (NA), west of the British Isles and south of Iceland. The AL resembles the positive phase of the East Atlantic (EA) pattern [*Barnston and Livezey*, 1987]. *Duchez et al.* [2016] describe an atmospheric configuration much like this regime in early summer 2015. The authors find that anomalously cold SSTs were present before the strong cyclonic anomaly over the NA appeared and propose that SSTs could have partially driven the anomalous atmospheric circulation, consistent with *Gastineau and Frankignoul* [2015]. Further, the EA pattern in summer can be hindcast by a multiple linear regression using Atlantic and tropical Indo-Pacific SSTs of the preceding winter and spring as predictors [*Iglesias et al.*, 2014]. This coupling of the atmosphere to the slowly-evolving boundary conditions is in fact one premise for seasonal predictability [*Palmer and Anderson*, 1994].

The European summer heat wave of 2003 was influenced by the presence of the AL regime in June [*Cassou et al.*, 2005]. This has been related to a Rossby wave train emanating from the Caribbean associated with diabatic heating anomalies caused by a northward shift of the Atlantic Intertropical Convergence Zone [*Black et al.*, 2004]. The existence of such a tropical-extratropical link is a second premise for the seasonal predictability of extratropical variability [*Shukla et al.*, 2000]. Teleconnections rely on the propagation of planetary-scale waves [*Liu and Alexander*, 2007] which are often generated by diabatic heating anomalies in the tropics [*Sardeshmukh and Hoskins*, 1988; *Trenberth et al.*, 1998; *Ding et al.*, 2011]. Rossby waves only propagate in sufficiently strong meridional potential vorticity gradients in a westerly background flow [*Hoskins and Ambrizzi*,

1993]. Despite these gradients being weakest in summer and the tropical easterlies extending further into the summer hemisphere, at least two summer Northern Hemisphere (NH) teleconnections have been identified [*Ding and Wang*, 2005; *Lin*, 2009; *Ding et al.*, 2011; *Saeed et al.*, 2014]. It is thus conceivable that the AL regime has a remote forcing from the tropics. This suggests further potential for the prediction of this mode and of extreme temperature and precipitation events related to it.

In this study, we shall recover the dominant modes of atmospheric summer variability from reanalysis data. While the first mode is the SNAO, the second mode - that we refer to as the Summer East Atlantic (SEA) mode - is related to the AL regime. We shall analyze the influence of the SEA-related circulation anomalies on surface climate in the NAE region. Further, we shall show that a tropical diabatic heating forcing of the extratropical atmospheric circulation can be established for the SEA and highlight the implications for the prediction of this part of the summer variability with the help of two seasonal hindcast experiments. In section 2, we describe the applied methodology and experiments. The results are presented in section 3 and summarized and discussed in section 4.

2. Methodology and Experiments

2.1. EOF Analysis

In order to identify the dominant modes of boreal summer (June, July, August, hereafter JJA) variability in the NAE sector, we apply an EOF analysis to ERA-Interim [*Dee et al.*, 2011] JJA seasonal mean 500 hPa geopotential height (z_{500}) anomalies relative to their

1979-2016 JJA climatological mean. As the focus is on interannual variability, anomalies are detrended prior to analysis. Following the suggestion of *Greatbatch and Rong* [2006], EOF analysis for the summer season is conducted for the region from 40°N-70°N, 90°W-30°E (hereafter: the NAE sector).

2.2. Seasonal Hindcast Experiments

The seasonal hindcasts were carried out with the atmospheric component of the European Centre for Medium-Range Weather Forecasts Integrated Forecasting System (ECMWF IFS) [*Dee et al.*, 2011], cycle 40r1. Nine ensemble members were initialized from ERA-Interim around the beginning of May for each year (1980-2014) and integrated until the end of August.

Two experiments were conducted that differ in terms of lower boundary conditions, i.e. SST and sea ice (SST/SI). While the OBS ensemble is forced globally with observed daily SST/SI from the HadISST data set, the CLIM ensemble is driven by daily climatological (1979-2014) SST/SI. For more details of the experimental strategy, see *Greatbatch et al.* [2012] and *Hansen et al.* [2017] (experiments OBS-NO and CLIM-NO therein).

3. Results

The two dominant EOFs explain approximately 35% and 18% of the JJA mean z_{500} variance in the 1979-2016 period, respectively. Only these first two modes are well separated from the higher order EOFs according to the criterion of *North et al.* [1982]. As

expected, the first EOF (Figure S1 in the supporting information) strongly resembles the SNAO as shown by *Folland et al.* [2009] despite their use of a different reanalysis product and different limits of their analysis domain. We do not discuss the SNAO any further here.

3.1. The Summer East Atlantic Pattern

The positive phase of the second EOF of JJA mean z_{500} anomalies in the NAE sector (Figure 1a) is accompanied by significant negative height anomalies over the NA south of Iceland and west of the British Isles extending northwestward over Greenland and the eastern North American continent. Anomalies of the opposite sign are centered around the Baltic Sea and extend over central and northern Europe. These circulation anomalies resemble the EA pattern of the boreal winter season [*Barnston and Livezey*, 1987]. Thus, we shall refer to the EOF2 of JJA mean z_{500} anomalies (Figure 1a) as the Summer East Atlantic (SEA) pattern and the corresponding Principal Component time series (Figure 1b, black bars) as the SEA index. Note that our definition of the SEA is different from the common definition of the EA pattern as the second rotated EOF of monthly z_{500} anomalies over the NH [*Barnston and Livezey*, 1987]. However, we find the SEA to be a robust feature of the summer circulation as it also arises when using height anomalies at other levels (surface to 200 hPa), over different periods of time, from NCEP/NCAR reanalysis or using monthly averages.

The regression of JJA z_{500} anomalies onto the SEA index (Figure 1c) exhibits significant SEA-related z_{500} anomalies also in extratropical regions outside of the NAE sector. These alternate in sign zonally and indicate that the SEA pattern is part of a circumglobal wave train. This notion is further supported by projecting the meridional wind component at 200 hPa (v_{200}) onto the SEA index (Figure 1d). At this level, the SEA is accompanied by significant meridional wind anomalies throughout most of the NH extratropics with the exception of eastern Asia and the western North Pacific. A wave number analysis of the v_{200} regression pattern reveals that the dominant zonal wave number is $k = 5$. Over the eastern North Pacific, North America and the North Atlantic, the major anomalies coincide with the climatological mean position of the NH summer jet stream (not shown) indicating that the SEA mode corresponds to a meandering of the jet.

3.2. SEA Impact on Precipitation and Surface Temperature in the NAE Sector

The regression of JJA surface temperatures onto the SEA index (Figure 1e) indicates a strong interannual relationship between surface temperature and the SEA mode in the NAE region and its immediate vicinity. In this area, the strongest cold (warm) anomalies coincide with the largest negative (positive) height anomalies (cf. Figure 1c and e). In case of a temperature control through warm (cold) air advection by the anomalous geostrophic flow however, we would expect the main temperature anomalies to occur where the SEA-related height gradients are strongest. Thus, the advective effect appears to be weak, which is supported by regressing temperature advection onto the SEA index (Figure S2). Instead, the spatial coincidence of temperature and height anomalies associated with the

SEA suggests a radiative control. The mechanism works such that positive (negative) temperature anomalies are caused by an increase (decrease) in local solar radiation and surface sensible heating that results from a decrease (increase) in cloud cover in response to anomalous sinking (rising) motions in the main anticyclonic (cyclonic) anomalies of the SEA pattern. This process has been suggested to cause the surface temperature anomalies associated with the SNAO [*Folland et al.*, 2009] and is investigated in detail by *Pfahl and Wernli* [2012]. The regression of total cloud cover (tcc) onto the SEA index (Figure S3) does not exhibit significant SEA-related anomalies over the NA. However, in the eastern part of the NAE sector, the significant tcc reduction associated with the positive SEA phase supports the proposed process.

As an example for the influence of the SEA on surface temperature, we consider the temperature measured at Hamburg, Fuhlsbüttel [*DWD*, 2017]. Its JJA mean (Figure 1b, blue line) is significantly correlated with the SEA index, which explains about 26% of its variance. This is more than is explained by the SNAO (approx. 21%). Furthermore, we find the 95th percentile of daily maximum temperatures (T_{DX95}) in high SEA index (¿ 1 standard deviation) summers to be 1.1°C higher than T_{DX95} for all summers pointing to an influence of the SEA on temperature extremes.

The precipitation signal associated with the SEA mode is weak in most of the NAE region (Figure 1f). Exceptions to this are the significantly enhanced rainfall west of the British Isles and the significantly reduced precipitation around the Baltic Sea. These

latter negative precipitation anomalies are in line with the SEA-related negative tcc and positive surface temperature anomalies (Figure 1e). This corroborates the importance of the aforementioned radiative control around the Baltic Sea.

3.3. Tropical Forcing of the SEA

Surface temperature and precipitation significantly covary with the SEA index in the tropics (Figures 1e and f). Regression coefficients are highest in the tropical central to eastern Pacific where warm SST anomalies and increased precipitation coincide with a positive SEA index. Over Central America and in the western tropical Atlantic on the other hand, relatively dry conditions and cold surface temperature anomalies accompany the positive SEA phase. A lagged regression of May precipitation onto the SEA index confirms that the rainfall anomalies in these areas are already present in spring (Figure S4). Diabatic heating associated with tropical precipitation anomalies can generate a Rossby Wave Source (RWS) that can induce tropical-extratropical teleconnections [*Sardeshmukh and Hoskins*, 1988]. To test if such a teleconnection associated with precipitation anomalies in these areas can be found, we introduce the Pacific-Caribbean Dipole (PCD) index. The PCD (Figure 1b, orange line) is defined as the normalized difference in precipitation averaged over a Pacific region (10°N-20°N, 180°-110°W) minus the precipitation averaged over the Caribbean (10°N-25°N, 85°W-65°W), indicated by the black boxes in Figure 1f. Note however, that the following results are not sensitive to the exact choice of the regions. They even remain valid when precipitation is replaced by SST. The PCD index is correlated with the SEA index at 0.56 (significant at the 99%-level) for the 1980-2014

period, suggesting a link between the two and showing that the PCD explains 31% of the variance in the SEA. Precipitation in the Pacific box explains 30% of SEA variance while the Caribbean part explains 12%.

In the regression of ERA-Interim JJA mean z_{500} onto the PCD index (Figure 2a), there is a pronounced pattern of height anomalies that alternate in sign zonally, reminiscent of a stationary wave train of zonal wave number 5. This wave train emanates from the central North Pacific, stretches over the North American continent, the NAE and northern Asia and thus almost spans the entire NH. Only over East Asia and the western North Pacific no significant height anomalies associated with the PCD can be found. Inside the NAE sector this structure projects strongly onto the SEA indicated by the high pattern correlation of 0.87, although the SEA amplitude is somewhat larger. Even over the entire NH, the wave train is similar to the SEA regression of z_{500} in Figure 1c. The emergence of the wave train in the height field related to tropical precipitation anomalies is an important indicator of the presence of a physical connection between the SEA mode and diabatic heating anomalies in the tropical central Pacific and west Atlantic. The results are further supported by the regressions of the RWS (for a definition see Section 2 of the supporting information) at 200 hPa onto the PCD and SEA indices (Figure S5). Both regression patterns generally agree and exhibit sources of cyclonic (anticyclonic) vorticity upstream of the main negative (positive) height anomalies of Figure 2a. The strongest RWS anomalies lie in the vicinity of the climatological NH summer jet stream, which can

act as a waveguide for Rossby waves [*Hoskins and Ambrizzi*, 1993].

To further corroborate the relevance of the tropical precipitation anomalies as a driver for the SEA mode, we redo the PCD regression with all ensemble members of OBS and CLIM (Figures 2b and c). There is a wave train in both ensembles that resembles the one in ERA-Interim to some degree even though both have smaller amplitudes. The regression in OBS projects strongly onto the SEA pattern while the centers of action are shifted eastwards in CLIM. Furthermore, the wave train in OBS over Eurasia loses similarity with the one from ERA-Interim, suggesting that extratropical SSTs anchor the wave train in OBS to be in a similar place as in ERA-Interim. The projection of the detrended OBS ensemble mean z_{500} anomalies onto the SEA pattern is correlated with the SEA index at 0.43 (statistically significant at the 95% level). For CLIM, the correlation is not significant (0.27). Furthermore, the fraction of SEA variance explained by the PCD in the ensemble mean of CLIM is only 2% while it is much closer to the observed value (26%) in the ensemble mean of OBS where it amounts to 25%. This indicates that a good representation of SST variability is crucial for a successful simulation of interannual SEA variability. These results generally support the previously proposed forcing mechanism of the teleconnection by tropical diabatic heating anomalies but also indicate a role for lower boundary forcing in other regions, a topic we discuss further in Section 4.

The averaging regions of the PCD are located in an area that is heavily influenced by the El Niño-Southern Oscillation (ENSO). It is thus conceivable that ENSO has an effect

on the SST and diabatic heating anomalies that induce the wave train. As an index for ENSO activity, we choose normalized ERA-Interim SST averages over the Niño3.4 region [*Trenberth and NCAR*, 2016], which we here call the N34 index. Correlating the monthly N34 index with the JJA PCD index (Figure 3) reveals that developing El Niño (La Niña) events tend to coincide with positive (negative) PCD anomalies thus forcing the positive (negative) SEA phase. This can be supported by regressing JJA z_{500} onto the N34 index of the following winter (DJF), which results in a wave train pattern much like the one in Figures 1c and 2 (Figure S6). This suggests that part of the SEA variability is accounted for by the developing ENSO phase. Indeed, lagged correlation values very similar to those in Figure 3 are obtained when the PCD index is replaced by the SEA index (Figure S7). The results presented above are not sensitive to excluding single years from the analysis.

3.4. The European Summer of 2015: Heat Wave under the Influence of the SEA?

It has been suggested that the most extreme European summer heat waves since the 1980s, in particular the 2015 one, were driven by cold NA SST anomalies [*Duchez et al.*, 2016]. Based on the results of our study, we argue that the excitation of the SEA mode by tropical diabatic heating anomalies could have been a dominant driver of the 2015 heat wave. Firstly, we note that the SEA index in that year exceeds one standard deviation making 2015 the 3rd strongest positive event in the 1979-2016 record (Figure 1b). Additionally, the 2015 JJA z_{500} anomalies (Figure S8) project well onto the SEA pattern despite some differences in the details of the wave train emanating from the tropical eastern Pacific from that shown in Figure 2a. Furthermore, the JJA mean PCD reaches its

highest positive value in the ERA-Interim record (Figure 1b, orange line) and its monthly anomalies are continuously above one standard deviation from April to September 2015 (not shown). This is also consistent with the developing strong El Niño that reached its peak in winter 2015/16 [*McPhaden*, 2015]. The coincidence of these factors points to the tropical-extratropical connection presented here being a factor in the dynamics of the European heat wave of 2015. It is further conceivable that the SST anomalies in the NA have contributed to the timing and intensity of this extreme event [*Duchez et al.*, 2016]. Such a conclusion is consistent with the comparison between OBS and CLIM discussed earlier.

4. Summary & Discussion

In this study, we have identified the SEA pattern, a mode of boreal summer atmospheric variability in the Euro-Atlantic region that is distinct and clearly separated from the dominant summer regime, the SNAO. Here, the SEA is defined as the second EOF of ERA-Interim JJA mean z_{500} anomalies from 1979-2016 in the North Atlantic-European (NAE) sector where it explains 18% of the seasonal mean variance (SNAO: 35%).

Some previous studies have considered low-frequency variability patterns in the boreal summer season other than the SNAO [*Cassou et al.*, 2005; *Ding et al.*, 2011; *Saeed et al.*, 2014; *Ghosh et al.*, 2017]. The closest resemblance is found between our study and that of *Cassou et al.* [2005]: their AL regime strongly resembles the positive phase of the SEA mode. They show that the occurrence of this regime significantly enhances the probabil-

ity of extreme temperatures in France. Other studies link a similar circulation anomaly pattern to single extreme summers [*Black et al.*, 2004; *Duchez et al.*, 2016]. Here, we present evidence that under the positive SEA, the seasonal mean surface temperatures are elevated while precipitation on average is reduced over central and northern Europe due to a decrease in cloud cover. It is conceivable that under these conditions, the probability of a heat wave is enhanced. However, the mechanisms of how the SEA impacts the extremes of the temperature and precipitation distributions have yet to be investigated systematically. Our results imply that the seasonal prediction of extreme events in the NAE region could strongly benefit from an improved representation of the SEA variability in models.

The potential for a better simulation of the SEA is also promising: We were able to show that the SEA is the NAE part of a tropical-extratropical teleconnection pattern in the summer NH. This teleconnection manifests as a stationary Rossby wave train of zonal wave number 5 originating in the North Pacific where it is associated with significant anomalous upper tropospheric divergent flow that acts as a wave source. The altered divergent flow is a response to anomalous convection in the central Pacific just north of the equator and anomalies of the opposite sign in the Caribbean. In fact, the wave train containing the SEA pattern can be recovered by regressing JJA mean height anomalies onto the PCD - a dipole index that quantifies the difference in precipitation between these regions. The tropical rainfall anomalies are the result of changes in SST that accompany a developing ENSO event such that a positive (negative) PCD is observed in summers

before the peak of El Niño (La Niña) (Figure S9). The tropical SST forcing of the teleconnection is further supported by two seasonal hindcast experiments. The full ensemble of an atmospheric model forced with observed SSTs (OBS) exhibits a PCD-related wave train in phase with the tropical-extratropical teleconnection in the reanalysis, though notably weaker in magnitude. Furthermore, the ensemble mean of OBS has significant skill in reproducing the interannual SEA variability in the reanalysis. One reason for this could be that the ensemble mean of OBS reproduces the observed precipitation anomalies as a result of the specified SSTs. This link between the extratropical SEA mode and developing ENSO-related SST anomalies has strong implications for the boreal summer seasonal prediction in the NAE sector. As the tropical large-scale circulation is predictable with inherently longer lead times than the extratropical atmosphere [*Palmer and Anderson*, 1994], a seasonal forecast of the SEA-related atmospheric summer variability could become a realistic objective. Testing for the presence of the teleconnection mechanism in a seasonal forecast model as well as statistical hindcasting of the SEA remain for future work.

It is worth pointing out that the PCD-related wave train is strikingly similar to the western Pacific-North America (WPNA) pattern [*Ding et al.*, 2011]. This structure arises as the second most dominant mode of joint boreal summer tropical precipitation and extratropical 200 hPa height variability from the NCEP/NCAR reanalysis. Especially over the eastern North Pacific and North America the similarity is strong. *Ding et al.* [2011] attribute the occurrence of the WPNA to a forcing by diabatic heating anoma-

lies over the Philippine Sea associated with the western North Pacific summer monsoon (WNPSM), which is part of the East Asian summer monsoon system and thus related to the Pacific-Japan pattern [*Sun et al.*, 2010]. Furthermore, they find the WPNA to appear in summers following the peak of an ENSO event. Both, the forcing and the ENSO relationship are in contrast to our results despite the apparent similarity in the teleconnection patterns. Further work is needed to resolve the role of a WNPSM forcing for the SEA.

There are studies putting forward an Atlantic SST forcing of SEA-like circulation anomalies [*Gastineau and Frankignoul*, 2015; *Duchez et al.*, 2016]. Although we do not examine this connection in detail here, our results do not contradict a possible influence. In fact, we do see the Atlantic SST tripole in months preceding the SEA (Figure S10), which is consistent with the results of *Gastineau and Frankignoul* [2015]. With our experiments however, it is not possible to disentangle the influences of NA SSTs and of tropical Pacific and Caribbean SSTs. The PCD-related wave train across the NA in OBS is in a similar place as in ERA-Interim, while the PCD-related wave train in the experiment with climatological SST/SI (CLIM) is shifted eastwards. This suggests that realistic SSTs, as in OBS, lock the extratropical wave train to the right phase, possibly even acting as a positive feedback to the atmospheric circulation anomalies.

Acknowledgments. ERA-Interim data was obtained from the ECMWF. CMAP data is provided by the Climate Prediction Center and downloaded from the Climate Data Guide. Temperature observations at Hamburg Fuhlsbüttel come courtesy of the German

Weather Service (DWD). We also want to acknowledge the ECMWF for providing the model and allowing access to their computer facilities for the model simulations used in this work. We thank Thomas Jung who carried out the model runs. Support from the German Federal Ministry of Education and Research (BMBF) through MiKlip2, subproject 01LP1517D (ATMOS-MODINI) is gratefully acknowledged. Finally, we are also grateful for continuing support from GEOMAR. All data used in this paper are available from the corresponding author. We thank two anonymous reviewers for their helpful comments.

References

Barnston, A. G., and R. E. Livezey (1987). Classification, Seasonality and Persistence of Low-Frequency Atmospheric Circulation Patterns. *Mon. Wea. Rev.* 115, 1083–1126

Black, E., M. Blackburn, G. Harrison, B. Hoskins, and J. Methven (2004). Factors contributing to the summer 2003 European heatwave. *Weather* 59 (8), 217–223

Cassou, C., L. Terray, and A. Phillips (2005) Tropical Atlantic influence on European heat waves. *J. Clim.* 18, 2805–2811

Coumou, D., and S. Rahmstorf (2012). A decade of weather extremes. *Nat. Clim. Chang.* 2 (7), 491–496

Dee, D. P., S. M. Uppala, A. J. Simmons, P. Berrisford, P. Poli, S. Kobayashi, U. Andrae, M. A. Balmaseda, G. Balsamo, P. Bauer, P. Bechtold, A. C. M. Beljaars, L. van de Berg, J. Bidlot, N. Bormann, C. Delsol, R. Dragani, M. Fuentes, A. J. Geer, L. Haimberger, S. B. Healy, H. Hersbach, E. V. Hólm, L. Isaksen, P. Kållberg, M. Köhler, M. Matricardi, A. P. Mcnally, B. M. Monge-Sanz, J. J. Morcrette, B. K. Park, C. Peubey, P. de Rosnay, C. Tavolato, J. N. Thépaut, and F. Vitart (2011). The ERA-Interim reanalysis:

Configuration and performance of the data assimilation system. *Quart. J. Roy. Meteor. Soc.* 137 (656), 553–597.

Ding, Q., and Wang, B. (2005). Circumglobal teleconnection in the Northern Hemisphere summer. *J. Clim.* 18 (17), 3483–3505

Ding, Q., B. Wang, J. Wallace, and G. Branstator (2011). Tropical-extratropical teleconnections in boreal summer: Observed interannual variability. *J. Clim.* 24 (7), 1878–1896.

Dole, R., M. Hoerling, J. Perlwitz, J. Eischeid, P. Pegion, T. Zhang, X. W. Quan, T. Xu, and D. Murray (2011). Was there a basis for anticipating the 2010 Russian heat wave?. *Geophys. Res. Lett.* 38 (6), L06702

Dong, B., R. Sutton, L. Shaffrey, and L. Wilcox (2016). The 2015 European Heat Wave in "Explaining Extremes of 2015 from a Climate Perspective". *Bull. Amer. Meteor. Soc.* 97 (12), S57–S62

Duchez, A., E. Frajka-Williams, S. A. Josey, D. G. Evans, J. P. Grist, R. Marsh, G. D. McCarthy, B. Sinha, D. I. Berry, and J. J.-M. Hirschi (2016). Drivers of exceptionally cold North Atlantic Ocean temperatures and their link to the 2015 European heat wave. *Environ. Res. Lett.* 11 (7), 074004

DWD Climate Data Center (CDC): Historische monatliche Stationsbeobachtungen (Temperatur, Druck, Niederschlag, Sonnenscheindauer, etc.) für Deutschland, Version v005, 2017.

Folland, C. K., J. Knight, H. W. Linderholm, D. Fereday, S. Ineson, and J. W. Hurrell (2009). The summer North Atlantic oscillation: Past, present, and future. *J. Clim.* 22 (5), 1082–1103

Gastineau, G., and C. Frankignoul (2015). Influence of the North Atlantic SST variability on the atmospheric circulation during the twentieth century. *J. Clim.* 28 (4), 1396–1416

Ghosh, R., W. A. Müller, J. Baehr and J. Bader (2017). Impact of observed North Atlantic multidecadal variations to European summer climate: a linear baroclinic response to surface heating. *Clim. Dyn.* 48 (11-12), 3547–3563

Greatbatch, R. J., and P.-P. Rong (2006). Discrepancies between different northern hemisphere summer atmospheric data products. *J. Clim.* 19 (7), 1261–1273

Greatbatch, R. J., G. Gollan, and T. Jung (2012). Factors influencing Northern Hemisphere winter mean atmospheric circulation anomalies during the period 1960/61 to 2001/02. *Quart. J. Roy. Meteor. Soc.* 138 (669), 1970-1982

Hansen, F., R. J. Greatbatch, G. Gollan, T. Jung, and A. Weisheimer (2017). Remote control of North Atlantic Oscillation predictability via the stratosphere. *Quart. J. Roy. Meteor. Soc.* 143 (703), 706–719

Hoskins, B., and T. Ambrizzi (1993). Rossby Wave Propagation on a Realistic Longitudinally Varying Flow. *J. Atmos. Sci.* 50 (12), 1661–1671

Hurrell, J., and C. Deser (2009). North Atlantic climate variability: The role of the North Atlantic Oscillation. *J. Mar. Syst.* 78 (1), 28–41

Iglesias, I., M. N. Lorenzo, and J. J. Taboada (2014). Seasonal Predictability of the East Atlantic Pattern from Sea Surface Temperatures. *PLoS ONE* 9 (1), e86439

Lin, H. (2009). Global Extratropical Response to Diabatic Heating Variability of the Asian Summer Monsoon. *J. Atmos. Sci.* 66 (9), 2697–2712

Liu, Z., and M. Alexander (2007). Atmospheric Bridge, Oceanic Tunnel, and Global Climatic Teleconnections. *Rev. Geophys.* 45 (2), 2005RG000172

McPhaden, M. J. (2015). Playing hide and seek with El Niño. *Nat. Clim. Chang.* 5 (9), 791–795

North, G., T. Bell, and R. Cahalan (1982). Sampling Errors in the Estimation of Empirical Orthogonal Functions. *Mon. Wea. Rev.* 110 (7), 699–706

Palmer, T., and D. Anderson (1994). The prospects for seasonal forecasting - A review paper. *Quart. J. Roy. Meteor. Soc.* 120 (158), 755–793

Pfahl, S., and H. Wernli (2012). Quantifying the relevance of atmospheric blocking for co-located temperature extremes in the Northern Hemisphere on (sub-)daily time scales. *Geophys. Res. Lett.* 39 (12), L12807

Saeed, S., N. Van Lipzig, W. A. Müller, F. Saeed, and D. Zanchettin (2014). Influence of the circumglobal wave-train on European summer precipitation. *Clim. Dyn.* 43 (1), 503–515

Sardeshmukh, P., and B. Hoskins (1988). The Generation of Global Rotational Flow by Steady Idealized Tropical Divergence. *J. Atmos. Sci.* 45 (7), 1228–1251

Shukla, J., J. Anderson, D. Baumhefner, C. Brankovic, Y. Chang, E. Kalnay, L. Marx, T. Palmer, D. Paolino, J. Ploshay, S. Schubert, D. Straus, M. Suarez, and J. Tribbia (2000). Dynamical Seasonal Prediction. *Bull. Amer. Meteor. Soc.* 81 (11), 2593–2606

Sun, X., R. J. Greatbatch, W. Park, and M. Latif (2010). Two major modes of variability of the East Asian summer monsoon. *Quart. J. Roy. Meteor. Soc.* 136 (649), 829–841

Trenberth, K. E. and National Center for Atmospheric Research Staff (Eds.) Last modified 02 Feb 2016. "The Climate Data Guide: Nino SST Indices (Nino 1+2, 3, 3.4, 4; ONI and TNI)." Retrieved from climatedataguide.ucar.edu.

Trenberth, K. E., G. Branstator, D. Karoly, A. Kumar, N. C. Lau, and C. Ropelewski (1998). Progress during TOGA in understanding and modeling global teleconnections associated with tropical sea surface temperatures. *J. Geophys. Res.* 103 (C7), 14291–14324

Wulff, O. (2017). Summer Variability in the North Atlantic-European region. Master Thesis. Christian-Albrechts-Universität Kiel, Kiel, Germany, URI: http://eprints.uni-kiel.de/39467/

Xie, P., and P. Arkin (1997). Global Precipitation: A 17-Year Monthly Analysis Based on Gauge Observations, Satellite Estimates, and Numerical Model Outputs. *Bull. Amer. Meteor. Soc.* 78 (11), 2539–2558

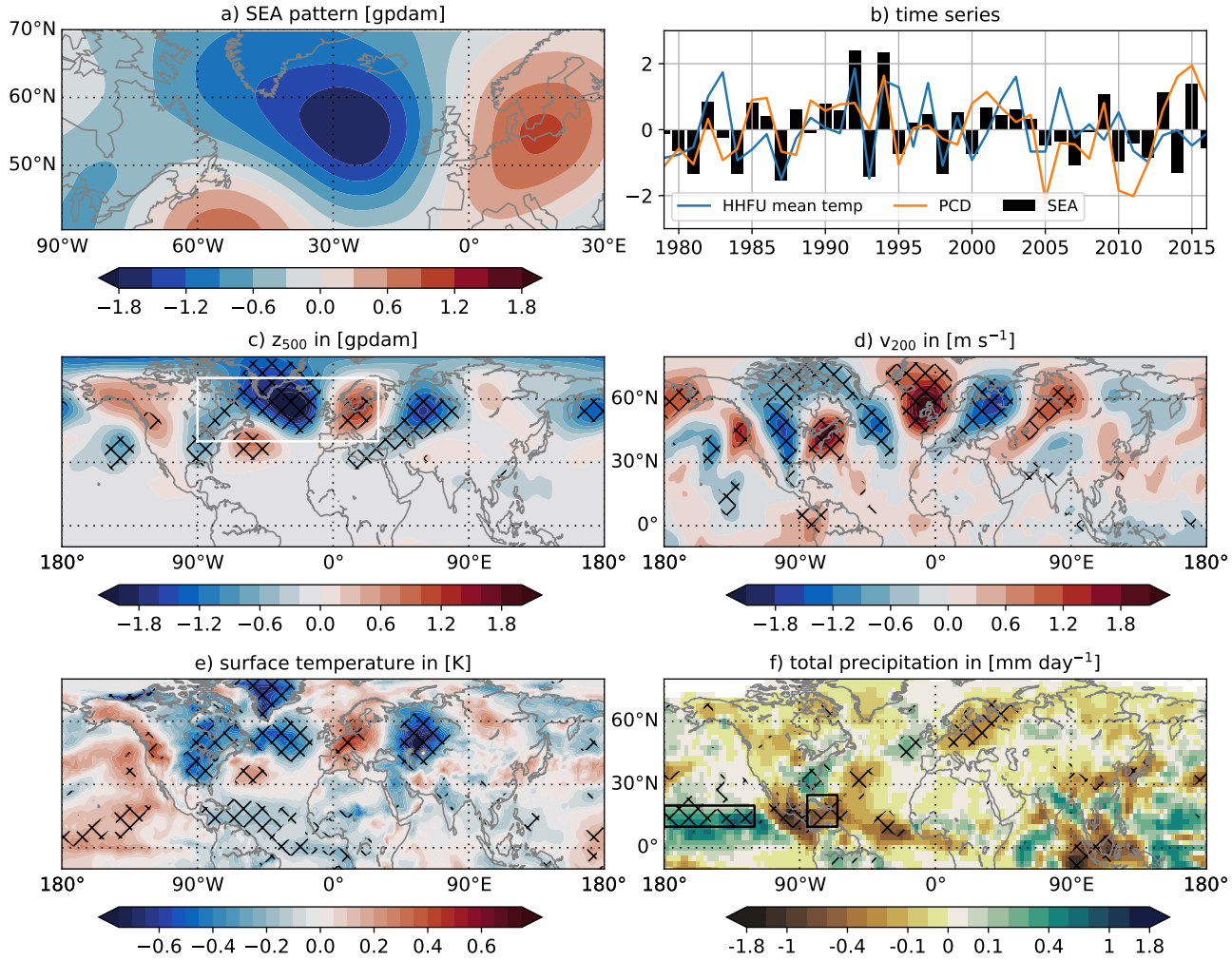

Figure 1. a) The SEA pattern as defined in the text; b) time series of the SEA index, the PCD (see Section 3.3 for details) and JJA temperature in Hamburg (HHFU); c-e) regressions of detrended ERA-Interim (1979-2016) JJA anomalies of (c) z_{500}, (d) v_{200}, (e) surface temperature (SST for ocean, 2m-temperature for land areas) and of (f) detrended CMAP [*Xie and Arkin*, 1997] JJA precipitation anomalies onto the SEA index as defined in the text. Note the non-linear scale in f. *Shading* in c to e shows the regression coefficient in the units given in the title of each panel per standard deviation of the SEA index. *Hatching* indicates regression coefficients significantly different from zero at the 95% level based on a t test. Definition region for the SEA mode indicated by white box in panel c); black boxes in panel f) indicate the PCD averaging regions.

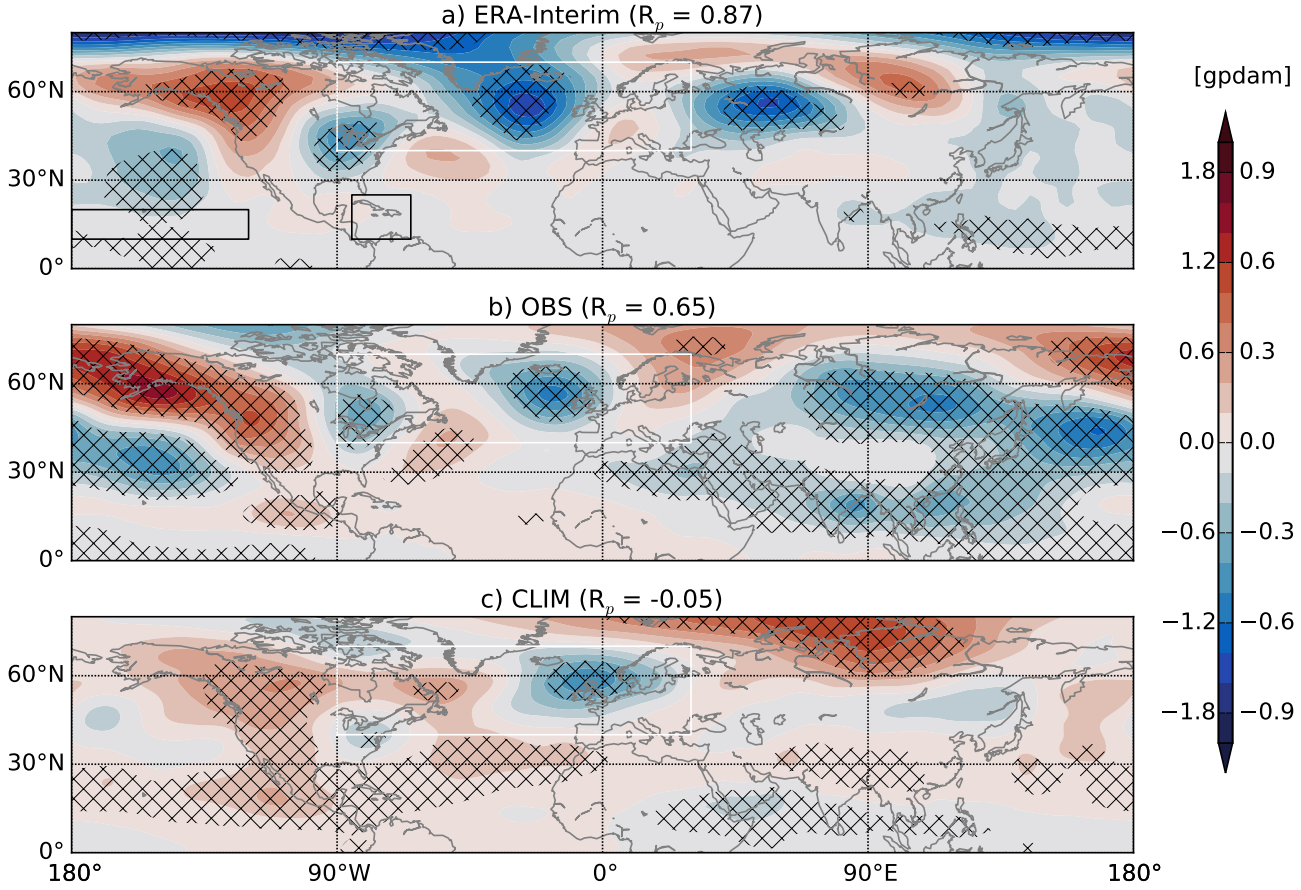

Figure 2. *Shading*: regression coefficients of JJA mean z_{500} anomalies (1980-2014) from (a) ERA-Interim onto the PCD index from CMAP and of (b) the OBS and (c) the CLIM ensemble onto the PCD index from the respective experiment in units of gpdam per standard deviation in PCD. Labels left of the color bar refer to (a), labels on the right apply to (b) and (c). All data were detrended prior to analysis. *Hatching* indicates where the regression coefficient is significantly different from zero at the 95% level based on a t test. Note that the significance threshold is much lower for (b) and (c) since the ensembles consist of 9 members resulting in a sample size 9 times as large as that of ERA-Interim. *Black boxes* in (a) show the PCD averaging regions, *white box* the NAE sector. R_p in each panel's title is the pattern correlation between the SEA pattern as defined in the text with the regression pattern inside the white box from the respective panel.

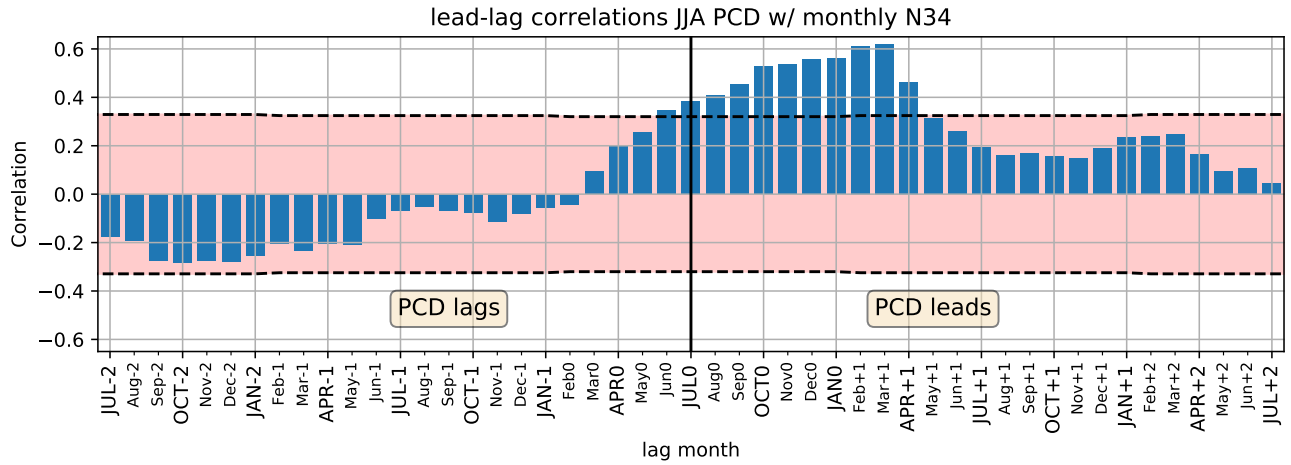

Figure 3. Correlations between the JJA PCD and the N34 index for different months. The maximum correlation (0.62) is found for Mar+1, i.e. between the JJA PCD and N34 in the following March. Correlations falling outside the red envelope are statistically significant at the 95% level.